University of Baghdad
College of Engineering
JE
JOURNAL OF ENGINEERING

Journal of Engineering
journal homepage: www.joe.uobaghdad.edu.iq
Number 3 Volume 26 March 2020

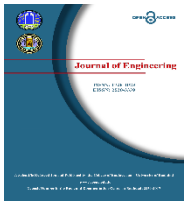

Mechanical and Energy Engineering

Evaluation of Fatigue Behavior of Epoxy Based Coatings used for Potable Water Storage Tanks

Haider Hadi Jasim*
Chemical Engineering Department, College of Engineering, Basrah University, Iraq
E-mail: raidhani73@yahoo.com

ABSTRACT

In this paper, three types of epoxy-based coatings (Polyamide, pure Polyamine, and Polyamine reinforced by glass-flake) used as a lining for potable water tanks were studied using experimental and finite element methods. Tensile, impact, and fatigue tests were conducted on uncoated and coated AISI 316 stainless steel. The test results show that the applied epoxy based coating improves the mechanical properties, increases of fatigue crack resistance, and enhance the dynamic fracture toughness. The fatigue crack propagation is influenced by the compositions of epoxy coating, and the glass-flake improves the coating resistance to fatigue crack propagation compared to other types.

Keywords: epoxy coating, fatigue, J-Integral, glass-flake, dynamic fracture toughness.

تقيم سلوك الكلل لطلاء الايبوكسي المستخدم في طلاء خزانات الماء الصالح للشرب

حيدر هادي جاسم
استاذ مساعد
كلية الهندسة- جامعة البصرة

الخلاصة

في هذا البحث، تم دراسة ثلاثة انواع من طلاءات الايبوكسي وهي البولي اميد، البولي امين النقي والبولي امين المقوى برقائق الزجاج المستخدمة في طلاء خزانات الماء الصالح للشرب باستخدام الطرق العملية وطريقة العناصر المحددة. اختبارات الشد والصدم والكلال اجريت على الصلب المقوى AISI 316 في حالة العينات المطلية وغير المطلية. النتائج بينت ان طلاء الايبوكسي يحسن الخواص الميكانيكية ويزيد مقاومة الصلب لشق الكلل ويحسن متانة الانكسار الديناميكية. انتشار شق الكلل يتأثر بتركيب طلاء الايبوكسي ورقائق الزجاج المضافة تحسن مقاومة انتشار شق الكلل مقارنة بالأنواع الاخرى.

الكلمات الرئيسية: طلاء الايبوكسي، الكلال، طريقة تكامل J ، رقائق الزجاج ، متانة الانكسار الديناميكية

*Corresponding author
Peer review under the responsibility of University of Baghdad.
https://doi.org/10.31026/j.eng.2020.03.02

Article received:3/3/2019
Article accepted:28/5/2019
Article published:1/3/2020

1. INTRODUCTION

The water storage tank is a reservoir that varies significantly in size, shape, and design and used to store the drinking water. Water tanks are found in all cities of Iraq, and they are used to supply potable water. There are three main types of drinking water tanks based on the location of the tanks; resting on ground, elevated water tank and underground tanks (**Kajarekar, 2018)**. Both types of tanks; resting on ground and elevated water ones are commonly used in Iraq provinces, which are built using the bolted, and the welding process of various types of stainless steel includes AISI 316, AISI 316L and ASTM 304. These types are used due to their high corrosion resistance and rigidity, (**Michael, 2011 and Tongue, 2015)**.

The most significant model of potable water tanks failure is attributed to either corrosion or fatigue problems. Epoxy coatings are the most commonly used to protect the potable water stainless steel from corrosion problems. The tanks are exposed to continuous operation of full and empty process by potable water and this exposition the stainless steel coats to stresses. These stresses can reach higher values when filled by drinking water and lower value when it's empty and thus making the coatings exposed to fatigue effects, (**Andres, 2016)**.

A number of reports have studied the fracture mechanics of steel and epoxy-based coating used for water tanks. (**Minoru, et al., 1985)**, tested and discussed the properties of several types of ultra-thick coatings including glass-flake coating, solventless epoxy coats, solventless polyurethane elastomer coats, and resin mortar coating. It has been discovered that the great preference for the offshore steel structures is used an ultra-thick, solventless epoxy coating due to its relatively stable film properties. (**Ebara et al., 1996),** estimated the corrosion fatigue behavior of the ballast tank steel coated by tar epoxy resin KA 32 (TMCP) by using the corrosion fatigue test for the plane round bar specimen with different thicknesses of tar epoxy resin coating. Their results indicated that there are improvements in corrosion fatigue strength in the lowest level of the stress, and the corrosion fatigue life was improved. (**Craig, 2005)**, studied stainless steel AISI 316L failures mode and corrosion problems in different environments. Their results showed that the failure of AISI 316L stainless steel is due to corrosion fatigue cracking in different environments under cyclical load. (**Gangloff, 2005)**, studied the effect of environment and corrosion pitting in the fatigue crack initiation. Their results showed that the pitting influences the growth rate of cracks and generally showed that the pitting increases the initiation of corrosion fatigue cracks. **(Mills and Eliasson, 2006)**, studied and reviewed the factors that influence initial cracks in marine cargo and water ballast tanks' structural frame. They show that as the flexibility of the coatings is reduced, the ability to withstand mechanical fatigue is reduced and resulting coating cracks are initiating. (**Mobin, et al., 2008),** presented the performance assessment of some fusion-bonded epoxy coatings underwater transmission line conditions. Their results show that all the coatings tested do not have any damage to the impingement, but show good adhesion and less blistering damage or color changes. (**Wang, et al., 2014),** investigated the effects of different oxide coatings on the fatigue performance of aluminum alloy 2024-T4. They found that the 2024-T4 aluminum alloy's fatigue performance could be improved by applying the coats on its surface. **(Sílvia, 2015),** used a finite element method to investigate the marine ship coating failure. They studied the influence of different parameters that contribute to the coating degradation behavior like temperature, loss of coating properties over time, humidity, environmental changes, impacts, the salinity of marine water, chemistry, and pH level. (**Momber, et al., 2016),** investigated the performance of six types of organic coating systems. The study focused on coating material, hardener, thickness of dry film, number of layers and method of application. The results show that the coatings change their response to impact loads at low temperatures and increase the adhesion of the coating in terms of pull-off strength.

In this paper, the experimental tensile, impact, and fatigue crack testing were conducted to study the effect of three types of epoxy-based coatings in mechanical properties and fatigue crack resistance of AISI 316L stainless steel used to construct drinking water tanks. The finite element software (Abaqus/CAE2016) and a J-integral program were used to estimate the rate of propagation of fatigue crack under different conditions.

2. EXPERIMENTAL METHODS

2.1 Types of Epoxy Based Coatings

Usually, the epoxy-based coatings used for drinking water tanks are free of solvents such as alcohol or phenol components. Three types of commercial Jotun epoxy coatings have been used to evaluate the tensile, impact and fatigue resistance, and one type has been used as a primer undercoats. These are the following coatings:

- Penguard Primer PM3192, epoxy primer based on a high molecular weight epoxy resin made by Jotun Henry Clark Ltd, UK. This type of coat was used as a primer under coots.
- Penguard HB, two-component (base and hardener) contains polyamide cured epoxy coating.
- Tank guard-412, two-component (base and hardener) contains polyamine cured epoxy coating.
- Penguard Pro GF; this type contains amine cured epoxy and reinforced by a glass flake.

The last three types of coatings are produced by Emirates Jotun Company of LLC Sharjah, U.A.E. Referring to these types of coatings, Penguard HB, Tankguard DW 412 and Penguard Pro GF as models A, B, and C, respectively.

2.2 The Coating Process

These epoxy-based coatings are applied in three main steps including surface preparation, surface cleaning and then applying coatings. After surface preparation and clean-up process, the Penguard primer PM3192 is applied directly onto the steel substrate by airless spray method. The primary function of the primer was to improve the overall adhesion of subsequently applied epoxy layer. Then, the three types of epoxy coatings are applied to the steel substrate at a sufficient coating film thickness by airless spray method. All the tensile tests and fatigue crack specimens after coatings were left to cure for two weeks at ambient condition (25^{o}C and atmosphere pressure), whereas the impact specimen was left to cure at different temperatures as discussed later.

The thickness of applied coatings is measured by a paint thickness meter manufactured by Gain Express Holdings Ltd, China and has an average value of less than 200 μm for all coating models, which is in the range of uses as given by the produced company.

2.3 Water Tank Material

The stainless steel grade AISI 316 is used in the experimental work. This type is broadly used for the constructing of water storage tanks in different provinces of Iraq. The AISI 316 stainless steel sheets are passive and exhibit a noble potential, so it has good corrosion resistance (**Basim, 2016)**. **Table 1** shows the basic chemical (mass %) composition.

Table 1. The mass % of constituent elements of AISI 316 Steel; (**Philip, 2003)**.

Element	Cr	C	Ni	N	Mn	Mo	Si	P
Mass %	0.08	0.08	14 Max.	0.1	2	2-3	0.75	0.045

2.4 Tensile Test

The tensile test has been conducted using the uniaxial tension test. In this test, the specimen is mounted in a machine and subjected to tensile forces. The magnitude of the specimen's gauge length increases will be recorded for a constant applied load. The results force-elongation data are converted to engineering stress-strain curve. The purpose of the test is to determine the tensile strength, yield strength, and elasticity module. The testing machine (Hounsfield SM1002) produced by Hounsfield-Company, UK, was used to perform a tensile test. **Fig. (1)A** shows the shape and dimensions of the tensile test specimen following (**ASTM E8M-01, 2001**). **Fig. (1) B to E** shows the specimens before and after coating by the three types of coatings. A total number of 4 specimens, one uncoated, and three specimens coated by the three types of coatings were used for tensile testing.

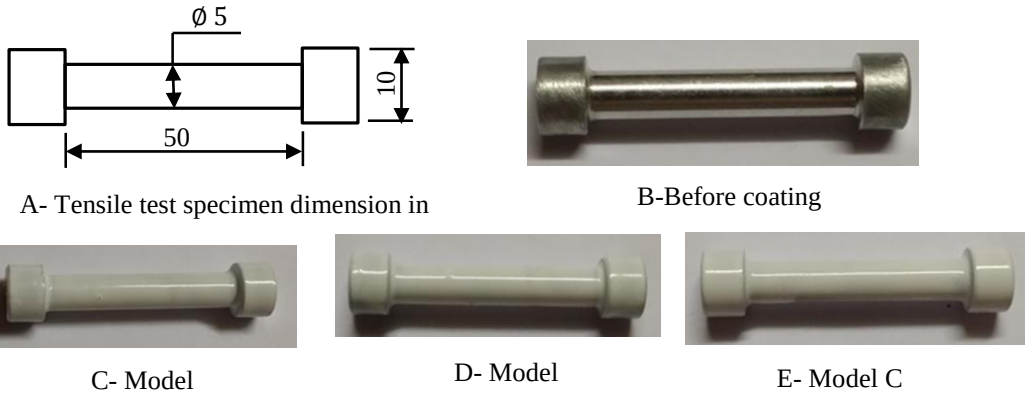

A- Tensile test specimen dimension in

B-Before coating

C- Model

D- Model

E- Model C

Figure 1. Tensile test specimen before and after coatings.

2.5 Impact Test

Based on standard (**ASTM E23-07a, 2011)**, the Charpy V-notch specimens were machined from a plate to standard size (10 x 10 x 55) in mm. The shape and size of the specimen are shown in **Fig. (2) A**. The dynamic fracture toughness (J_{Id}) is obtained using the specimens having the same size as shown in **Fig. (2) A**, but it has a pre-cracked of 2 mm in the V notch according to standard (**ASTM E399-90, 1997**). **Fig. (2) B to E** show specimens before and after coats. The specimens were tested at temperatures of 10, 20, 30, 40 and 50ºC. A total number of 20 specimens coated by the three types of coating models were used for Charpy impact testing (one, for each cure temperature), and five specimens of the uncoated stainless steel AISI 316 was used. The machine INSTRON WOLPERT PW30 has 250 kN load and capacity 300 J is used for testing. The dynamic fracture toughness (J_{Id}) is obtained by using the maximum load energy method from the following equation, (**Xinping and Yaowu, 1996)**:

$$J_{Id} = \frac{2\,E_m}{B(W-a_o)} \quad (1)$$

Where,

E_m: Maximum load of energy.

B: Thickness of specimen in m.

W: Width of the specimen in m.

a_o: Initial length of crack 2 mm.

The standard deviation (SD) of tensile test and Charpy impact data are obtained by using the following formula, (**Stanisław, 2014)**:

$$SD = \sqrt{\frac{(X-\overline{X})}{N}} \quad (2)$$

Where,

$\overline{X}$: The mean of dataset.

N: The number of dataset.

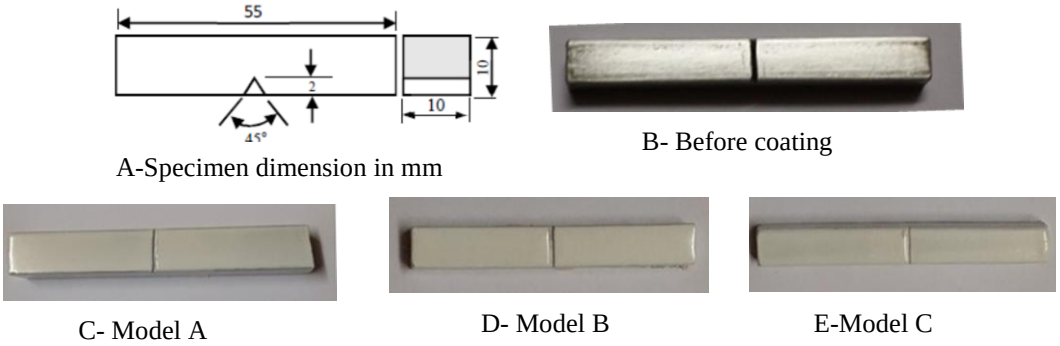

A-Specimen dimension in mm

B- Before coating

C- Model A

D- Model B

E-Model C

Figure 2. Specimens for Charpy impact test.

2.6 Fatigue Testing

The experiment fatigue cracks growth testing was conducted using a standard single-edge notched compact tension (CT) specimen according to standard (**ASTM E647-00, 1998)**. **Fig. (3) A** shows specimen shape and dimensions in mm. The specimen has 12.5 mm in thickness. The specimens before and after coatings by the three types of coats are shown in **Fig. (3) B to E**. The Bi-04-CP-310 universal testing machine produced by TCR Eng. Co. Pvt., India was used for achieving the fatigue test. A total number of three coated specimens and one uncoated stainless steel specimen were used for fatigue testing.

During the test, the specimen is subjected to a cyclic loading P, which causes the crack length to increase by increment which is recorded with the number of load cycles. The data acquired is presented in (a vs. N) curve. Many curves can be obtained by applying various magnitude of the loading cyclic for many various matching test specimens having the same primary crack length a_o, and the results are demonstrated in **Fig. (4)**.

To determine the crack growth change for each applied cycle *(da/dN)* from **Fig. (4)** using the secant technique. In this method, the slope of the straight line tangent of each curve is calculated by the following equation (**ASTM E647-00, 1998)**:

$$\frac{da}{dN} = \frac{\Delta a}{\Delta N} = \frac{a_{i+1}-a_i}{N_{i+1}-N_i} \quad (3)$$

Where,

da/dN: The rate of fatigue crack growth per cycle in (mm/cycle).

N: Number of cycles.

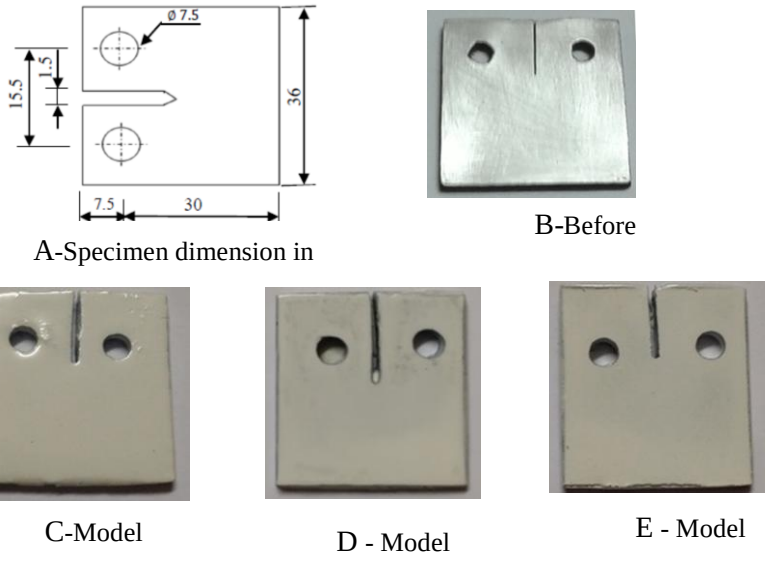

Figure 3. Compact tension specimen dimension and geometry before and after coats.

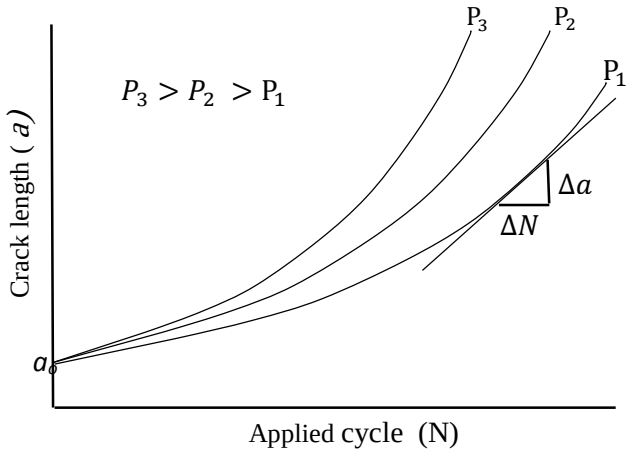

Figure 4. The crack length extensions vs. applied cycles.

The crack growth length through the load cycle applied was measured using a microscope that has an amplification of 100 times, then the stress intensity factor of uncoated and coated compact tension specimen was calculated by the following formula, (**Bower, 2009)**:

$$K = \frac{P}{B}\sqrt{\frac{\pi}{W}}\left[16.7\left(\frac{a}{W}\right)^{0.5} - 104.7\left(\frac{a}{W}\right)^{1.5} + 369.9\left(\frac{a}{W}\right)^{2.5} - 573.8\left(\frac{a}{W}\right)^{3.5} + 360.5\left(\frac{a}{W}\right)^{4.5}\right] \quad (4)$$

Where,

a: Crack length in mm.

P: Applied load in kN.

B: Thickness of the specimen in mm.

W: Width of the specimen in mm.

After calculating the stress intensity factor from **Eq.(3)**, the fatigue crack growth rate can be described by the Paris and Erdogan relationship as followers, (**Wengang and Jonas, 2013)**:

$$\frac{da}{dN} = C\,(\Delta K)^m \quad (5)$$

And

$$\Delta K = K_{max.} - K_{min.} \quad (6)$$

Where,

C and m: Paris parameters.

K_{min} and $K_{max..}$: Minimum and Maximum values of a stress-intensity factor in (MPa. $\sqrt{m}$).

3. FINITE ELEMENT ANALYSIS

The finite element method (FEM) is a numerical method used to obtain the stress intensity factor (K_I) in the open mode (mode I) of elastic compact tension specimen, (**Rafa'a and Hayder, 2015)**. The program (Abaqus/CAE 2016) software, as well as the J-integral program, were used to obtain stress intensity factors. **Fig. (5)** shows the specimen mash modeled using 3-nodes element in 2-D plane strain problems. It's assumed the specimen is anisotropic and the specimen has a unit thickness in FEM analysis. Symmetric boundary conditions were applied in the (Abaqus/CAE2016) software. The displacement is restricted to all nodes of **Fig. (5)** located along the x-axis, while the displacement is considered free at nodes located along crack length. Since there are two holes in the compact tension specimen, incremental increasing loads are applied only to the nodes located along the y-axis on these holes.

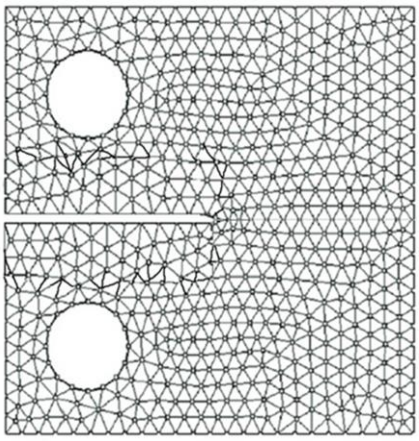

Figure 5. Finite element mesh using 3 nodes triangular element.

J-Integral represents the rate of energy release and can be computed by integral of independent path line around crack tip, (**Rege and Lemu, 2017)**. For analyzing of compact tension specimen during fatigue crack growth rate, since the integral path independence of J-integral is not evaluated during unloading condition, this use of the J-integral range (ΔJ) as the fracture parameter. During cyclic loading, the J-integral range (ΔJ) is computed and defined as the difference between maximum values of J-integral during loading applied and minimum values unloading condition. The relationship between J-integral range and stress intensity factor range is given as follows, (**Nirpesh and Kumar, 2013)**:

$$\Delta J = \frac{(\Delta K)^2}{E} \quad (7)$$

Where,
E: Modulus of elasticity in MPa.
ΔK: Range of stress intensity factor in MPa.$\sqrt{m}$.
For two-dimensional crack problems in case of opening mode (mode I) of linear elastic fracture mechanics, the J-integral is defined as (**Nirpesh and Kumar, 2013)**:

$$J = \int_{\Gamma} W_i dy - \int_{\Gamma} T^t \frac{\partial u}{\partial x} ds \quad (8)$$

The strain energy is computed using the following formula (**Sicelo, 2013)**:

$$W_i = \int_0^{\varepsilon} \underline{\sigma}^t d\underline{\varepsilon} = \frac{1}{2} \sigma^t \underline{\varepsilon} \quad (9)$$

Where,
J: Energy release rate in N/mm.
W_i: Strain energy density in J/m^3.
T: Traction vector.
ds: Element differential along the contour.
u_i : Displacement vector.
t: Transpose of a matrix.
Γ: The path of contour.
x, y: Cartesian axis that parallel and vertical to the crack tip.
$\underline{\varepsilon}$: Strain vector.
$\underline{\sigma}$: Stress vector.

4. RESULTS AND DISCUSSION

4.1 Tensile Test Results

The obtained results from the tensile test are represented as shown in **Fig. (6)** in the form of the stress-strain curves. The mechanical properties: tensile strength (S_u), yield strength (S_y) and modulus of elasticity (E) of AISI 316 stainless steel in cases of uncoated and coated by the three types of Jotun coatings were obtained from the stress-strain curves of **Fig. (6**) and these properties are listed in **Table (2)** with its standard division calculated using **Eq.(2)**. The inflection of applied tensile stress at 0.034 strains for AISI 316 stainless steel and 0.035 strains for all coated specimens were observed from **Fig. (6)**. At this point of inflection, the cracking begins to initiate and spread as observed microscopically during the conduct of the tensile test. The yield strength at this point of inflections was calculated from the stress-strain curves. The applied tensile forces to the uncoated specimen of AISI 316 stainless steel increases with increased applied load until the strain becomes 0.33, then it starts to decrease until the specimen fracture occurs.
As seen in **Fig. (6)**, the tensile properties of the coated specimens are enhanced, and this can be attributed to that the coated epoxy layers improved and increased the strength of specimens to have applied force during the tensile test.
In model C, the reinforcement of glass-flakes reduces the segmental movement of the epoxy coating chains and improves the cross-linking density of the coating. This improves the elongation and compression resistance of epoxy coats. Also, it reduces the extent of damage and flaw in the epoxy coats during conduct the tensile test. So, the mechanical properties of this type of coating are improved compared to the other two types of coatings.

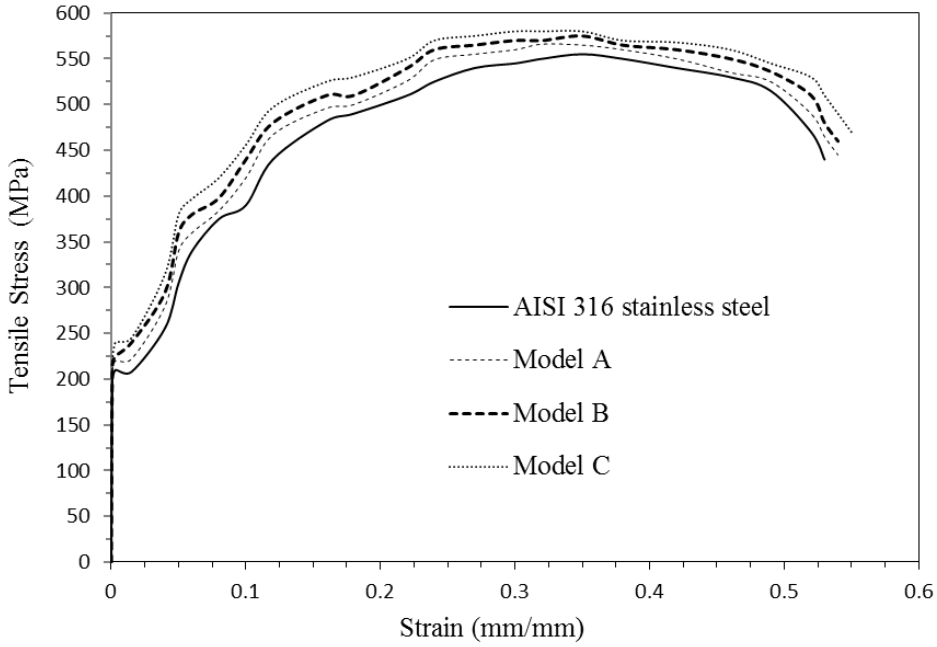

Figure 6. Tensile curves of uncoated and coated specimen.

Table 2. Mechanical properties of uncoated and coated steel obtained from the tensile test.

Properties	Uncoated		Model A		Model B		Model C	
	Measured	SD	Measured	SD	Measured	SD	Measured	SD
S_u (MPa)	550	8.125	566	0.125	570	1.875	579	6.375
S_y(MPa)	200	4.375	205	1.875	211	1.125	219	5.125
E (GPa)	190	5.250	194	3.250	202	0.750	216	7.750

4.2 Charpy Test Results

The Charpy tests have been performed at different temperatures: 10, 20, 30, 40 and 50°C and the results are shown in **Table 3** with its standard division calculated using **Eq.(2).** As seen from **Table 3**, at different temperatures, the AISI 316 stainless steel coated by Model C has the highest values of impact energy. This has been attributed to the fact that during the impact testing the epoxy coatings can withstand and absorbed some of the impact energy. In Model C, the impact energy is increased by large values compared to the uncoated AISI 316 stainless steel, and the significant difference becomes small at high temperatures. Model A has lowered impact energy values, and Model B displays moderate values.

Rising the temperature effects on model A coats compositions consisting of amide cured pure epoxy and becoming softer and less tough than the other two coats. Model C is reinforced by a glass flake that increases the properties of cohesion and adhesion between the components themselves and with the surface of stainless steel, resulting in high rigidity of the epoxy coating compared to other types. As the temperature increases, less cohesive force between the epoxy molecules and the epoxy group leads to a reduction in the value of the energy needed to break the specimen. Model B consists of polyamine having moderate cohesive strength values between the

epoxy molecules and the epoxy group, resulting in moderate fragility resulting in moderate impact energy values.

Table 3. Results of the Charpy impact test at different temperatures.

Temperature (°C)	Uncoated		Impact energy J					
			Model A		Model B		Model C	
	Measured	SD	Measured	SD	Measured	SD	Measured	SD
10	127	4.25	133	1.25	137	0.75	145	4.75
20	114	4.5	118	2.5	123	0.01	137	7.00
30	104	4.87	107	3.37	113	0.37	131	8.63
40	97	4.62	100	3.12	106	0.13	122	7.87
50	86	5.25	92	2.25	98	0.75	110	6.75

The dynamic fracture toughness at different temperature conditions corresponding to the energy measured using pre-cracked specimens was calculated using **Eq.(1)** are summarized in **Table 4**. As indicated in **Table 4**, the value of J_{Id} obtained at low temperatures was higher than that values obtained at high temperatures. Also, the applied coatings are increased the dynamic fracture toughness of AISI 316 stainless steel. It is noticed that the dynamic impact energies obtained in **Table 4** are less compared to values given in **Table 3**. This attributed to the effect of pre-cracked in specimens, which contribute to reducing the impact energy.

Table 4. Dynamic fracture toughness (J_{Id}) of uncoated and coated steel.

Temperature (°C)	Uncoated		Model A		Model B		Model C	
	Impact energy (J)	J_{Id} (kJ/m^2)	Impact energy (J)	J_{Id} (kJ/m^2)	Impact energy (J)	J_{Id} (kJ/m^2)	Impact energy (J)	J_{Id} (kJ/m^2)
10	114	430.2	118	454.3	126	475.5	138	520.8
20	112	422.6	115	434.0	119	449.1	129	486.8
30	98	369.8	102	384.9	107	403.8	116	437.7
40	91	343.3	96	362.3	103	388.7	109	411.3
50	81	305.7	85	320.8	88	332.1	93	350.8

4.3 Fatigue Test Results

The load applied during fatigue test ranges from 2 to 25 kN by the increasing values of 0.4 kN incremental for each cycle until a fracture occurs. The crack length at each loading cycle was measured during the test, and the collected data are drawn, as shown in **Fig.7**. All models illustrated in **Fig.7** have the same behavior and demonstrate a significant change in the fatigue crack extension values at a final cycle. Model C of epoxy-based coating has the best crack extension resistance compared to other models of coatings.

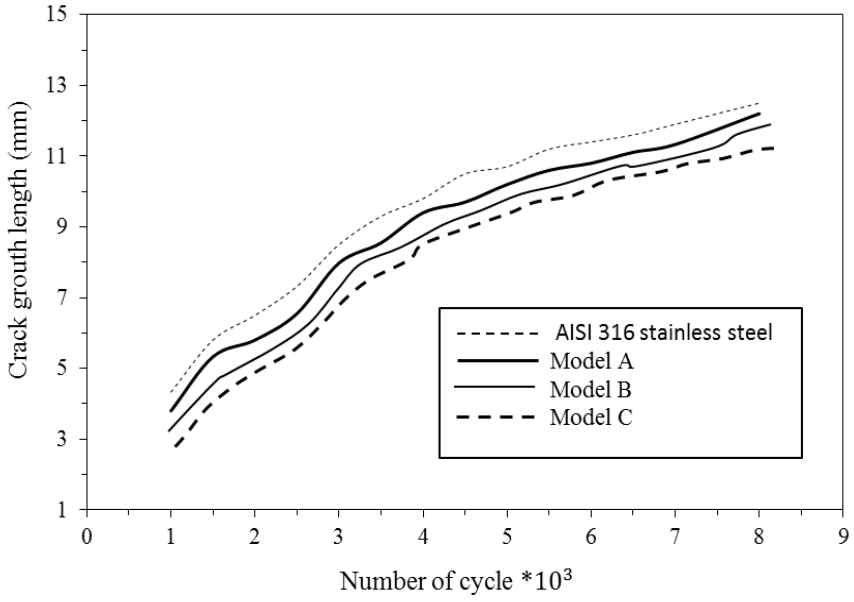

Figure 7. Comparison of crack growth length vs. No. of cycles of uncoated and coated steel

To obtain the J-Integral values representing the energy release rate of crack propagation the data obtained from FEM using (Abaqus/CAE2016) software program that includes displacement stresses, and strains were input into J-integral program. For the four contours, the J-Integral values were taken into account around the crack tip for varying crack length with different loads of displacement. **Eq.(3)** was used to evaluate the maximum stress intensity factors. The minimum stress intensity factor is considered equaling to zero ($K_{min.}$= 0) since consideration is given to the case where there was no loading. The values of ΔK are computed using **Eq.(6)** as the difference $K_{max.}$- $K_{min.}$. The comparisons of ΔK vs. the length of crack acquired from FEM and experimental fatigue test are illustrated in **Fig. (8)**.

From the fatigue test, the maximum stress intensity factor was obtained by measuring the length of crack for each load applied to the compact tension specimen and by using **Eq.(4)**, while $K_{min.}$ = 0 (case no applied loading). As shown in **Fig. (8**), good agreement between experimental and FEM results. The rate of crack growth is not uniform increases, and they are not linear with a rise of ΔK. **Fig. (9)** shows the da/dN (increasing the length of the crack for each applied fatigue cycle) vs. (ΔK) for coated and uncoated stainless steel. Using the tangential method, from **Fig. (8)** and by a used of Eq.(3), the da/dN values were acquired based on number of cycles recorded during the fatigue test after each 2 mm extension crack space. The applied epoxy coating on the AISI 316 stainless steel increases the fracture toughness ($K_{max.}$ values) compared to the values acquired of uncoated AISI 316 stainless steel.

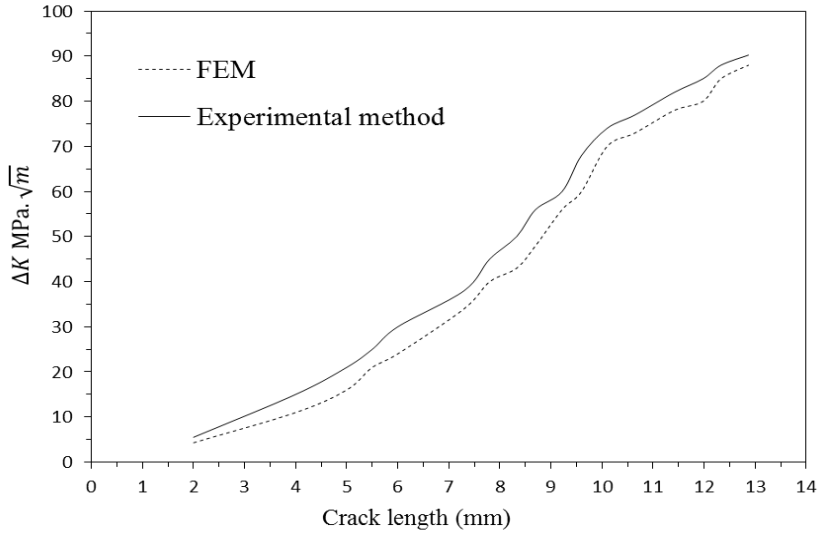

Figure 8. ΔK vs. crack length obtained from FEM and experimental.

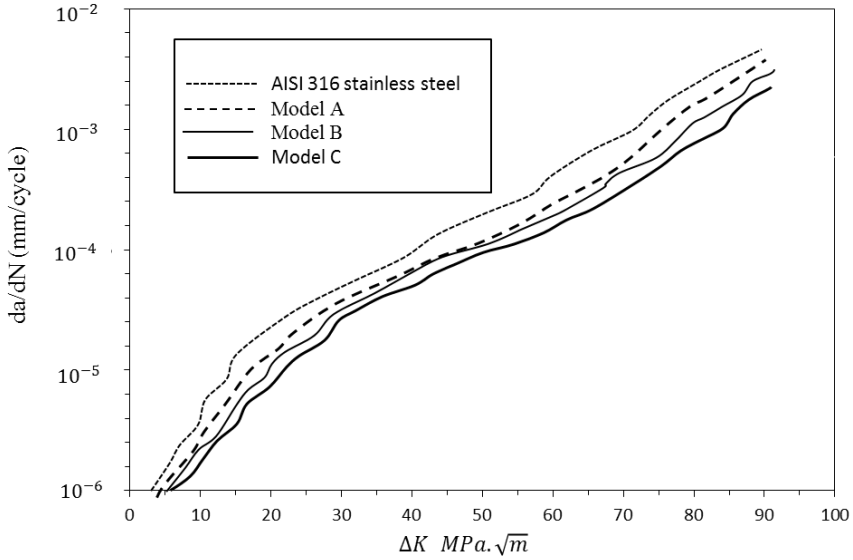

Figure 9. Crack growth rate vs. ΔK for AISI 316 steel and coated by the coatings.

The relationship between the rate of crack growth da/dN of epoxy-based coatings and the stress intensity factor range (ΔK) in opening mode (Mode-I) is given by **Eq.(5),** i.e. the Paris power law. The drawing of log (da/dN) vs. log (ΔK) of **Eq.(5)** for each stress ratio, the values of Paris's constants (m), and (C) were established from the curves by taking slopes of each curve. **Table 5** summarizes the values of (m) and (C) for case of coated and uncoated stainless steel.

The parameter of Paris law as a function of the pure mechanical damage is useful in determining the acceleration of increasing cracks based on crack growth rate. It is also noted that these constant reduces for models A, B, and C, respectively, compared to uncoated AISI 316 stainless steel. This reflects that rate of crack propagation in general decreases when applied the epoxy-based coatings.

Table 5. Paris power law parameters acquired from Fig. 9.

Constants	Uncoated	Model A	Model B	Model C
m	2.618	2.60	2.57	2.52
C	$6*10^{-8}$	$5.92*10^{-8}$	$5.8*10^{-8}$	$5.7*10^{-8}$

Compared to polyamide coats, the polyamine epoxy coats have more resistance to crack propagation, and this can be attributed to the different factors related to each type of coat composition. Amine cured pure epoxy resins have high cross-links density due to having multiple epoxide groups likes (alkyl group, vinyl groups, aryl groups, etc.); this leads to high resistance to crack propagation when compared with polyamide curing pure epoxy coats. In addition to that, the amine cured epoxy coats have higher molecular weight and viscosity; it has higher functionality (refer to the number of resin's chemical backbone site reactions). The larger the epoxide functionality of the amine cured epoxy, the greater its crosslink density and this makes their resistance to fatigue crack greater to that having by the amide cured pure epoxy. In comparison with polyamide polyamine epoxy coats, the glass-flake in model C of coats enhances the components bonds and increases the rates of crack propagation resistance. Flake-glass spread in various directions, and some of flake glass becomes a perpendiculars bridge to the direction of crack spread in the internal coatings.

5. CONCLUSIONS

Tensile, impact, and Fatigue behaviors of three types of epoxy coating were studied and discussed in detail. The following conclusions are obtained from the previous discussion:
1-Good agreements are obtained between the results of fatigue crack tests and the finite element method.
2-The applied of epoxy coatings on AISI 316 stainless steel improved the fatigue crack resistance irrespective the composition of each type of epoxy-based coatings.
3-Polyamine reinforced by glass-flake is more resistance to the propagation of fatigue crack compared to pure polyamine and polyamide coatings.
4-The coatings applied to enhance the dynamic fracture toughness, and as temperature increases, the dynamic fracture toughness decreases.

ACKNOWLEDGMENTS

The author would like to thank the staff engineer of the Material Eng. Dept. of Basrah University for their help during prepare the specimen and conducted the fatigue test.

6. REFERENCES

- Kajarekar B., Gangurde A., Gunjal K., Bhalchim D., and Yewale D. S., 2018, *Comparative estimation of underground water tank and elevated storage tank of Junnar*, International Journal of Advance Engineering and Research Development, 5(4), pp.1-7.

- Michael L. Doolittle, 2011, *A Comparison of ultra-long-life coating systems for water storage tanks*, Report of Selecting and Sourcing Coating Systems for Water Tanks, 7-12, A JPCL eBook, Technology Publishing Company, USA.

- Tongue W., 2015, *Investigation of the fracture behavior of epoxy-based water ballast tank coatings under static and fatigue loadings*, Ph.D. Thesis, University of Cranfield, UK.

- Andres E. R. A., 2016, *Failure pressure and fatigue analysis of the API 12Fshop welded flat bottom tanks*, M.Sc. Thesis, Purdue University, Indiana.

- Minoru K., Kotaro Y., Toshikuni K., Teruo M., Kyoichi K., and Yoshiaki S., 1985, *Examination of heavy-duty, ultra-thick coating systems for offshore steel structures*, Transactions ISIJ, 25(1), pp.1-8.

- Ebara R., Yamada Y., Kino H., Tada M., Hashimoto K., Imajo Y. and Fushim A., 1996, *Corrosion fatigue behavior of tar epoxy resin coated ship structural steel, Journal of the Society of Nava*, 1996(180), pp.521-530.

- Craig BD, 2005, *Material failure modes-part I: a brief tutorial on fracture, ductile failure, elastic deformation, creep and fatigue*, JFAP 2005, 4(5), pp.39-45.

- Gangloff R. P., 2005, *Environmental cracking-corrosion fatigue, Corrosion Tests and Standards: Application and Interpretation*, ASTM, R. Baboian (Ed.), West Conshohocken, PA, pp.302–321.

- Mills G. and Eliasson J., 2006, *Factors influencing early crack in marine cargo and ballast tank development*, Journal of Protective Coatings and Linings, 23(2), pp.1-13.

- Mobin M., Malik A. U., Andijani I. N., Al-Muaili F., M. Al-Hajri, Ozair G. and Mohammad N. M. K., 2008, *Performance evaluation of some fusion-bonded epoxy coatings underwater transmission line conditions*, Progress in Organic Coatings, 62(4), pp.399-375.

- Wang X. S., Guo X. W., Li X. D., and Dge Y., 2014, *Improvement on the fatigue performance of 2024-t4 alloy by synergistic coating technology*, Materials, 7(1), pp.3533- 3546.

- Sílvia C. Guerreiro de Sousa, 2015, *Coating breakdown analysis of steel plates in marine structures*, M.Sc. Thesis, Naval Architecture, and Marine Engineering, Tecnico Lisboa, France.

- Momber A. W., Irmer M., and Gluck N., 2016, *Performance characteristics of protective coatings under low-temperature offshore conditions, Part 1: Experimental set-up and corrosion protection performance*, Cold Reg. Sci. Technol., 127(1), pp.76–82.

- Basim O. Hasan, Naseer A. Al-habubi and Samar S. Hussien, 2016, *Galvanic corrosion of carbon steel-stainless steel couple in sulfuric acid under flow conditions*, Journal of Engineering, 8(22), pp.159-174.

- Philip D. Harvey, 2003, *Engineering properties of steels*, Eighth-Edition, American Society for Metals, Metals Park, OH, USA.

- ASTM E8M-01, 2001, *Standard test methods for tension testing of metallic materials*, Report of ASTM International, Conshohocken, PA, USA.

- ASTM E23-07a, 2011, *Standard test methods for notched bar impact testing of metallic materials*, Report of ASTM International, Pennsylvania, USA.

- ASTM E399-90, 1997, *Standard test methods for plane-strain fracture toughness of metallic materials*, Report of ASTM International, West Conshohocken, PA, USA.

- Xinping Z. and Yaowu S., 1996, *Comparative studies of several methods to determine the dynamic fracture toughness of nuclear pressure vessel steel A508 CL3, with Charpy-size specimen*, Int. J. of Fracture, 81, pp.195-204.

- Stanisław A., Jerzy B. and Bozena K., 2014, *Estimating the uncertainty of tensile strength measurement for a photocured material produced by additive manufacturing*, Metrology and Measurement Systems, 21(3), 553-560.

- ASTM E647-00, 1998, *Standard test method for measurement of fatigue crack growth rates*, Report of ASTM International, West Conshohocken, PA, USA, 1-19.

- Bower A. F., 2009, *Applied Mechanics of Solids*, 1st Edition, CRC Press Taylor and Francis Group, USA.

- Wengang M. and Jonas R., 2013, *Analysis of fatigue crack initiation and propagation in ship structures*, 13th International Conference on Fracture, June 16–21, Beijing, China, pp.1-10.

- Rafa'a M. Abbas and Hayder J. Shakir, 2015, *Finite element investigation on shear lag in composite concrete-steel beams with web openings*, Journal of Engineering, 3(21), pp.11-33.

- Rege K. and H. Lemu, 2017, *Review of fatigue crack propagation modeling techniques using FEM and XFEM*, Materials Science and Engineering, 276, pp.1-16.

- Nirpesh V. and Kumar R., 2013, *Review on fatigue-crack growth and finite element method*, International Journal of Scientific and Engineering Research, 4(4), pp.833-843.

- Sicelo P. Goqo, 2013, *A computational study of compact tension and double torsion test geometries*, Ph.D. Thesis, Department of Mathematics and Applied Mathematics, Faculty of Science, University of Cape Town, South Africa.